Ambient Backscatter in Reality: Does Illuminator Signal Structure Matter?

Georgios Vougioukas and Aggelos Bletsas
School of Electrical and Computer Engineering, Technical University of Crete, Chania 73100, Greece
e-mail: gevougioukas@isc.tuc.gr, aggelos@telecom.tuc.gr

***Abstract*—Motivated by the extensive use of simplified models in the recent ambient backscatter literature, this work will demonstrate the importance of utilizing realistic models when deriving appropriate detectors. For this purpose, two recent works on ambient backscatter will be evaluated under realistic channel models, accounting for all communication parameters. It is shown that assuming a complex normal illuminator (i.e., ignoring illuminator's signal structure) leads to significant performance losses compared to explicitly considering illuminator's modulation (e.g., FM). Based on FM illumination, the importance of the latter is further highlighted by deriving a high performance, fully non-coherent sequence detector. In most cases, switching techniques (e.g., SBPSK) are shown to outperform conventional techniques (OOK), at the expense of increased complexity.**

I. Introduction

Besides its most known application on commercial RFID tags, communication using backscatter radio techniques has recently attracted a lot of interest for the development of ultra-low power wireless sensor networks (WSNs) [1] and internet-of-things (IoT) devices. In conventional radio communication, information is modulated on top of a locally-created RF carrier signal; instead, in backscatter radio, a tag modulates information on top of a signal impinging (from a distant transmitter) on its antenna, by altering the termination of the latter. An appropriate receiver is then used to recover tag's information from the reflected signals. If the receiver and the transmitter/RF illuminator are co-located, the setup is referred to as monostatic and it is the case of commercial, typical, RFID systems. On the other hand, if the RF illuminator and the receiver of the backscattered signals are geographically separated units, a bistatic setup is obtained [2], while a multistatic setup is considered when multiple RF illuminators are used [3]. This work considers a special case of bistatic backscatter radio, namely ambient backscatter.

In ambient backscatter, the RF illuminator is not a dedicated device that emits unmodulated RF signals; instead, modulated RF signals from ambient RF transmitters are exploited for the illumination of each tag's antenna. The first implementation of ambient backscatter tag-to-tag communication was given in [4], where illumination from ambient digital television (DTV) broadcasting stations was exploited. Illumination from FM radio stations was exploited for communication in [5], [6].

Theoretical studies on ambient backscatter communication have recently appeared in the literature. The repeating structure of an orthogonal frequency-division multiplexing (OFDM) illuminating signal was exploited in [7]. Detectors were derived using the central limit theorem (CLT) and assuming binary phase shift keying (BPSK) modulation at the tag, along with a form of differential signaling. Assuming that the samples of the illuminating carrier's complex envelope are drawn from a circularly symmetric complex Gaussian (normal) (CN) distribution, energy and maximum-likelihood (ML) detectors, for on-off keying (OOK) modulation at the tag, were given in [8], [9] (and references therein). Illumination from a phase shift keying (PSK) modulated source was also considered. Higher order, M-PSK modulation was considered in [10] and energy detectors along with symbol error rate (SER) closed form expressions and a prototype implementation were offered. Detailed surveys of current ambient backscatter literature can be found in [11], [12].

The main intention of this work is to highlight the importance of using realistic models when studying ambient backscatter. A significant portion of the literature ignores the underlying structure of the illuminating signal, in favor of simplified circularly symmetric complex Gaussian models. Such models may simplify derivation of appropriate detectors at the expense of significant performance loss, as will be shown subsequently. On the other hand, taking explicitly into account illuminator's signal structure can lead to increased performance gains, even when fully non-coherent techniques are employed. Besides simplified modeling of illuminator's signal structure, the vast majority of ambient backscatter literature overlooks important communication parameters (e.g., large scale fading). The signals involved are subject to significant path-loss (the illuminator may be far away from the tag) and this fact must be explicitly taken into account when deriving the signal model. Based on a signal model derived under realistic assumptions, the performance of detection techniques offered by recent ambient backscatter literature will be evaluated. Detectors derived under the umbrella of CN illumination will be also evaluated under different modulations. Significant performance gaps are shown to exist when considering realistic (vs simplified) signal models for ambient backscatter communication, showcasing the importance of incorporating all the involved parameters along with realistic modeling of illuminator's signal. Additionally, a fully non-coherent detector aimed at FM-based ambient backscatter communication will be offered and evaluated.

Backscatter principles, OOK, shifted-BPSK (SBPSK) modulations and their respective signal models are provided in

978-1-5386-8088-9/19/$31.00 ©2019 IEEE

Sec. II. The detection techniques for each modulation are given in Sec. III, while the evaluation/comparison is given in Sec. IV. Finally, work is concluded in Sec. V.

II. Signal Model

A. Tag Operation

In backscatter communications, a device/tag varies the impedance terminating its antenna. Under illumination from an RF wave and assuming a load causing imperfect termination, the antenna reflects (part of) the impinged wave. By altering the loads terminating the tag's antenna, the characteristics of the reflected signal can be manipulated.

Considering the tag antenna-load system, the reflection coefficient can be defined as:

$$\Gamma_{\mathrm{i}} = \frac{Z_{\mathrm{i}} - Z_{\mathrm{a}}^{*}}{Z_{\mathrm{i}} + Z_{\mathrm{a}}},\ i = 0, \ldots, \mathrm{M}_{\text{loads}} - 1, \tag{1}$$

where Z_{i} the load terminating the antenna, Z_{a} the antenna's impedance and $\mathrm{M}_{\text{loads}}$ the number of utilized loads. For example, if $Z_{\mathrm{i}} = Z_{\mathrm{a}}^{*}$ then the tag antenna-load system will be matched and, ideally, all the power will be delivered on Z_{i}; on the contrary, if $Z_{\mathrm{i}} \neq Z_{\mathrm{a}}^{*}$ then reflection will occur that depends on Z_{i}. Different modulation schemes can be achieved by carefully selecting different Z_{i} and methods for alternating between them. Given that no mixers, filters or amplifiers are required, tag implementation can be manifested with ultra-low power hardware designs [12], sparking increased research interest on backscatter communications.

The tag's complex baseband signal can be expressed as [2]:

$$\mathsf{x}(t) = A_{\mathrm{s}} - \Gamma(t)\,, \tag{2}$$

where A_{s} is the antenna's structural mode, a (load-independent) parameter determined by antenna's characteristics. The value of the reflection coefficient at time instant t is given by $\Gamma(t)$. Thus, a specific modulation using backscatter principles requires careful design of $\Gamma(t)$.

For backscatter OOK, two loads at the tag are necessary in order to end up with two discrete values for $\Gamma(t)$. Consecutively, the tag's signal for the duration of the nth bit can be expressed as:

$$\mathsf{x}_{\text{OOK}}^{i_{\mathrm{n}}}(t) = A_{\mathrm{s}} - \Gamma_{i_{\mathrm{n}}},\ i_{\mathrm{n}} \in \{0, 1\}\,, \tag{3}$$

where $t \in [\mathrm{nT}_{\text{bit}}, (\mathrm{n}+1)\,\mathrm{T}_{\text{bit}})$ with T_{bit} denoting the bit duration. Such operation can be implemented with an RF switch, two loads Z_0, Z_1 and a suitable controller. In order for bit "0" to be backscattered, the switch terminates the antenna at load Z_0 (resulting to reflection coefficient Γ_0) for T_{bit} seconds. Similarly, for backscattering bit "1", Z_1 is chosen.

Frequency-based modulation schemes can be realized by continuously alternating the loads at a specific rate. For example, backscatter binary FSK [2], [13] can be implemented by continuously switching between the loads (Z_0, Z_1) for a duration of T_{bit} seconds, using different switching rates, i.e., $F_{\text{sw},0}$ for backscattering bit "0" or $F_{\text{sw},1}$ for "1". The aforementioned operation can be mathematically described as follows:

$$\mathsf{x}_{\text{FSK}}^{i_{\mathrm{n}}}(t) = m_{\mathrm{dc}} + m_{\mathrm{tag}}\mathsf{cos}(2\pi F_{\mathrm{sw},i_{\mathrm{n}}} t + \Phi_{\mathrm{t},i_{\mathrm{n}}})\,, \tag{4}$$

where $t \in [\mathrm{nT}_{\text{bit}}, (\mathrm{n}+1)\,\mathrm{T}_{\text{bit}})$ and $\Phi_{\mathrm{t},i_{\mathrm{n}}}$ fixed phases introduced by tag's switching. Parameters $m_{\mathrm{dc}}, m_{\mathrm{tag}}$ are given below:

$$m_{\mathrm{dc}} = \left(A_{\mathrm{s}} - \frac{\Gamma_0 + \Gamma_1}{2}\right),\ m_{\mathrm{tag}} = \frac{2\,(\Gamma_0 - \Gamma_1)}{\pi}. \tag{5}$$

In this work, besides OOK, another switching-based technique will be compared, namely *shifted* (or *switched*) BPSK (SBPSK) [3], [14]. The latter is a combination of BPSK and FSK and the information is encapsulated in the phase of the tag's switching signal (the signal driving the RF switch), mathematically described as follows:

$$\mathsf{x}_{\text{SBPSK}}^{i_{\mathrm{n}}}(t) = m_{\mathrm{dc}} + m_{\mathrm{tag}}\mathsf{cos}(2\pi F_{\mathrm{sw}}\, t + \Phi_{\mathrm{t}} + \phi_{i_{\mathrm{n}}}(t))\,. \tag{6}$$

Information is encapsulated in $\phi_{i_{\mathrm{n}}}(t)$. In that way, assuming binary signaling with frequency F_{sw},

$$\phi_0(t) = \Phi_0,\ \phi_1(t) = \Phi_0 + \Delta\Phi, \tag{7}$$

with $t \in [\mathrm{nT}_{\text{bit}}, (\mathrm{n}+1)\,\mathrm{T}_{\text{bit}})$. Switching frequency F_{sw} is fixed/information independent. The constraints affecting the choice of F_{sw} can be found in [14]. Due to switching at a single rate F_{sw}, a single phase parameter Φ_{t} is considered. That phase is considered (for SBPSK) random but constant throughout the transmission of a packet.

When compared to OOK, schemes employing switching for their operation (e.g., FSK, SBPSK), will have increased tag power consumption (due to increased complexity) that scales linearly with the utilized switching frequency [15]. However, tags utilizing moderate switching frequencies (in the order of few MHz) can be implemented with power consumption in the μWatt range [14]. As will be shown below, switching-based techniques offer significant performance gains, compared to OOK.

B. Ambient Backscatter Wireless Signal Model

In conventional bistatic (e.g., [16]) or monostatic (e.g., Gen2 RFID) setups, the RF wave that illuminates the tag comes from a dedicated device, typically emitting unmodulated RF signals. In this work, a special case of bistatic backscatter radio is considered, namely ambient backscatter. In ambient backscatter, existing *modulated* signals are exploited for RF illumination. Those signals may come from FM radio stations, DTV broadcasting stations or other Marconi (i.e. conventional) transmitters in the environment.

The considered setup is shown in Fig. 1. In ambient backscatter, the RF illuminator may be located far away from the tag, while the tag-to-reader distance is limited in the order of a few meters [4], [6]. Thus, the signal model must take into account large-scale fading. Consecutively, a standard path-loss model [17] is considered for each link, depicted in Fig. 1:

$$L_{\mathrm{q}} = \left(\frac{\lambda}{4\pi d_0}\right)^{2} \left(\frac{d_0}{d_{\mathrm{q}}}\right)^{\nu},\ \mathrm{q} \in \{\mathrm{CT}, \mathrm{TR}, \mathrm{CR}\}\,, \tag{8}$$

where $\mathrm{CT}, \mathrm{TR}, \mathrm{CR}$ denote the carrier-to-tag, tag-to-reader and carrier-to-reader links, respectively, while d_{q} denotes the

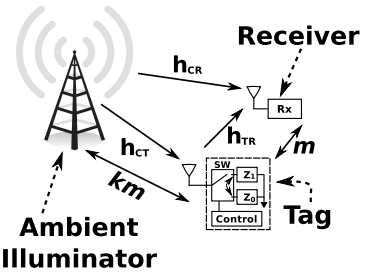

Fig. 1: Ambient backscatter communication setup; the signals involved are subject to significant path-loss (due to large distances) and fading across at least two links. These factors must be explicitly taken into account.

associated distance. Reference distance d_0 is set to 1 m, while ν denotes the path-loss exponent; for a carrier signal centered at F_c, wavelength is $\lambda = \frac{3\cdot 10^8}{F_\mathrm{c}}$.

Small-scale flat fading is assumed, with complex baseband channel gain given by:

$$h_\mathrm{q} = \alpha_\mathrm{q} \mathsf{e}^{-\mathrm{j}\phi_\mathrm{q}},\ \mathrm{q} \in \{\mathrm{CT}, \mathrm{TR}, \mathrm{CR}\}\,, \tag{9}$$

where $\alpha_\mathrm{q} \in \mathbb{R}_+$ and $\phi_\mathrm{q} \in [0, 2\pi)$. For the complex channel gains h_q it is assumed:

$$h_\mathrm{q} \sim \mathcal{CN}\left(\sqrt{\frac{\mathrm{k_q}}{\mathrm{k_q}+1}\sigma_\mathrm{h}^2}, \frac{\sigma_\mathrm{h}^2}{\mathrm{k_q}+1}\right), \tag{10}$$

where $\mathcal{CN}\big(\mu, \sigma^2\big)$ denotes the proper complex Gaussian distribution of mean μ and variance σ^2. Eq. (10) can be used to model both Rician and Rayleigh fading. Under Rician fading, factor $\mathrm{k_q}$ expresses the power ratio of the dominant path over the scattered paths ($\mathrm{k_q} > 0$). Rayleigh fading can be obtained by setting $\mathrm{k_q} = 0$. The tag is located close to the receiver and a strong line of sight path is probable. Thus, Rician fading is assumed for the tag-to-reader (TR). On the other hand, the ambient illuminator is typically located far from both the tag and the receiver/reader. Thus, the corresponding links (CT, CR) are potentially amenable to rich scattering conditions, so Rayleigh fading is assumed ($\mathrm{k_{CR}} = \mathrm{k_{CT}} = 0$).

The ambient illuminator/carrier emitter (CE) emits a modulated RF signal with complex baseband representation,

$$c(t) = \mathrm{m_c}(t)\, \mathsf{e}^{-\mathrm{j}(2\pi\Delta F_\mathrm{c} t + \Delta\phi)}, \tag{11}$$

where $\mathrm{m_c}(t)$ is the complex envelope of the illuminating carrier. The frequency and phase offsets between the ambient carrier and the receiver are modeled by ΔF_c and $\Delta\phi$, respectively. $\Delta\phi$ is modeled as $\Delta\phi \sim \mathcal{U}\,[0, 2\pi)$, where $\mathcal{U}\,[a, b)$, denotes the uniform distribution in range $[a, b)$. The signal impinging at the tag's antenna is given by:

$$\begin{aligned} c_\mathrm{tag}(t) &= c(t)\,\sqrt{L_\mathrm{CT}}\,h_\mathrm{CT} \\ &= \sqrt{L_\mathrm{CT}}\,h_\mathrm{CT}\,\mathrm{m_c}(t)\,\mathsf{e}^{-\mathrm{j}(2\pi\Delta F_\mathrm{c} t + \Delta\phi)}. \end{aligned} \tag{12}$$

The signal at the receiver can be then expressed as [2], [14]:

$$\begin{aligned} \mathrm{y}(t) = \frac{1}{2}\Big(&\sqrt{L_\mathrm{CR}}\,h_\mathrm{CR}\,c(t) + \sqrt{L_\mathrm{TR}}\,h_\mathrm{TR}\,\mathrm{s}\,c_\mathrm{tag}(t)\,\mathsf{x}(t)\Big) \\ &+ \mathsf{w}(t)\,, \end{aligned} \tag{13}$$

where $\mathsf{w}(t)$ models the thermal noise at the receiver, s denotes the tag scattering efficiency and term $\frac{1}{2}$ is due to (assumed) homodyne processing at the reader. Assuming perfect carrier frequency offset (CFO) correction, the signal model for each considered case is given below.

1) Ambient Backscatter using OOK: When OOK is utilized at the tag's side, $\mathsf{x}(t)$ takes the form of Eq. (3) and the signal model of Eq. (13), for the duration of the nth bit, i.e., for $t \in [\mathrm{n}\mathrm{T_{bit}}, (\mathrm{n}+1)\,\mathrm{T_{bit}})$, becomes:

$$\begin{aligned} \mathrm{y}_\mathrm{OOK}^{i_\mathrm{n}}(t) = &\frac{1}{2}\mathsf{e}^{-\mathrm{j}\Delta\phi}\mathrm{m_c}(t) \\ &\times \left[\sqrt{L_\mathrm{CR}}\,h_\mathrm{CR} + \sqrt{L_\mathrm{CT}L_\mathrm{TR}}\,h_\mathrm{CT}\,h_\mathrm{TR}\,\mathrm{s}\,(A_\mathrm{s} - \Gamma_{i_\mathrm{n}})\right] \\ &+ \mathsf{w}(t)\,. \end{aligned} \tag{14}$$

In accordance to the considered study in [18], it is assumed that $\Gamma_1 = -1$ and $\Gamma_0 = 0$. Thus, assuming a sampling rate of $F_\mathrm{s} = 1/T_\mathrm{s}$, the model in Eq. (14) can be further simplified to:

$$\mathrm{y}_\mathrm{OOK}^{i_\mathrm{n}}[k] = \mathrm{y}_\mathrm{OOK}^{i_\mathrm{n}}(kT_\mathrm{s}) = \mathrm{m_c}[k]\,h_{i_\mathrm{n}} + \mathsf{w}[k]\,, \tag{15}$$

where $\mathsf{w}[k] \sim \mathcal{CN}\big(0, \sigma_\mathsf{w}^2\big)$ and:

$$h_{i_\mathrm{n}} = \begin{cases} \frac{1}{2}\mathsf{e}^{-\mathrm{j}\Delta\phi}\big(\sqrt{L_\mathrm{CR}}h_\mathrm{CR} + a_\mathrm{tag}A_\mathrm{s}\big)\,, & i_\mathrm{n} = 0, \\ \frac{1}{2}\mathsf{e}^{-\mathrm{j}\Delta\phi}\left[\sqrt{L_\mathrm{CR}}h_\mathrm{CR} + a_\mathrm{tag}\,(A_\mathrm{s}+1)\right], & i_\mathrm{n} = 1, \end{cases} \tag{16}$$

with $a_\mathrm{tag} = \sqrt{L_\mathrm{CT}L_\mathrm{TR}}\,h_\mathrm{CT}\,h_\mathrm{TR}\,\mathrm{s}$.

2) Ambient Backscatter using SBPSK: In a similar manner to the aforementioned OOK case, the model for SBPSK takes the following form [14]:

$$\begin{aligned} \mathrm{y}_\mathrm{SBPSK}^{i_\mathrm{n}}[k] = \frac{1}{2}\mathsf{e}^{-\mathrm{j}\Delta\phi}\mathrm{m_c}[k]\Big[&\sqrt{L_\mathrm{CR}}h_\mathrm{CR} + a_\mathrm{tag}m_\mathrm{dc} \\ &+ a_\mathrm{tag}m_\mathrm{tag}\mathsf{cos}(2\pi F_\mathsf{sw}\,kT_\mathrm{s} + \Phi_\mathrm{t} + \Phi_{i_\mathrm{n}})\Big] + \mathsf{w}[k]\,. \end{aligned} \tag{17}$$

III. Detection Techniques

As already stated, the goal of this work is to highlight the importance of realistic models, when dealing with ambient backscatter communication. Failure to do so, may lead to results which are hard to obtain under realistic conditions. In order to showcase that importance, three detection techniques will be compared, based on the signal models offered in Sec. II. As the vast majority of ambient backscatter literature [8], [9], [11], [7] assumes OOK modulation at the tag (due to ease of implementation), detection methods offered by a representative example of recent ambient backscatter literature [18], will be used on the model of Eq. (15). Besides, in [18], comparisons are made with previous related studies on the subject. For the switching scheme of Eq. (17), detection techniques offered in [14] will be used. Additionally, based on Eq. (17) and results of [14], a fully non-coherent detector will be offered, assuming FM illumination.

A. Detection of Backscatter OOK

1) OOK Detection under CN Illumination: In the first scenario, samples $\mathrm{m_c}[k]$ of $\mathrm{m_c}(t)$, are assumed to be drawn from a circularly symmetric complex Gaussian distribution, i.e., $\mathrm{m_c}[k] \sim \mathcal{CN}(0, 2P_{\mathrm{tx}})$, where P_{tx} the transmission power of the ambient illuminator. Under the CN assumption and based on Eq. (15), two hypotheses $\mathcal{H}_0, \mathcal{H}_1$ are formed [18]:

$$\mathcal{H}_{i_\mathrm{n}} : \mathbf{y}_{\mathrm{OOK}}^{i_\mathrm{n}} \sim \ \mathcal{CN}\big(0, \sigma_{i_\mathrm{n}}^2 \, \mathbf{I}_L\big) \, , \ i_\mathrm{n} \in \{0, 1\} \, , \tag{18}$$

where $\mathbf{y}_{\mathrm{OOK}}^{i_\mathrm{n}} = \left[\mathrm{y}_{\mathrm{OOK}}^{i_\mathrm{n}}[0], \ldots, \mathrm{y}_{\mathrm{OOK}}^{i_\mathrm{n}}[\mathrm{L}-1]\right]^{\mathrm{T}}$ and L is the oversampling factor, i.e., $L = T_{\mathrm{bit}}/T_{\mathrm{s}}$. Variances are given by:

$$\sigma_{i_\mathrm{n}}^2 = |h_{i_\mathrm{n}}|^2 2P_{\mathrm{tx}} + \sigma_{\mathsf{w}}^2. \tag{19}$$

Assuming perfect knowledge of parameters $\sigma_{i_\mathrm{n}}^2$, the maximum likelihood (ML) detector takes the form of the following decision rule [18]:

$$\delta(\mathbf{y}_{\mathrm{OOK}}) = Z \underset{>}{\overset{\mathcal{H}_0}{}} T_h^{\mathrm{CG/ML}}, \ \text{if } \sigma_0^2 > \sigma_1^2, \tag{20}$$

where $Z = ||\mathbf{y}_{\mathrm{OOK}}||_2^2$ and threshold $T_h^{\mathrm{CG/ML}}$ is given by:

$$T_h^{\mathrm{CG/ML}} = \frac{L\,\sigma_0^2\sigma_1^2}{\sigma_1^2 - \sigma_0^2} \ln \frac{\sigma_1^2}{\sigma_0^2}. \tag{21}$$

In the case of $\sigma_0^2 \leq \sigma_1^2$, an inversion of the decision is performed, i.e., $1 - \delta(\mathbf{y}_{\mathrm{OOK}})$.

2) OOK Detection under PSK Illumination: In the second scenario, samples $\mathrm{m_c}[k]$, are assumed to attain PSK modulation:

$$\mathrm{m_c}[k] = \sqrt{2P_{\mathrm{tx}}} \exp\left(\mathrm{j}\frac{2\pi l}{\mathrm{M_{PSK}}}\right), \ l = 0, \ldots, \mathrm{M_{PSK}} - 1, \tag{22}$$

where $\mathrm{M_{PSK}}$ is the modulation order. It is noted that term 2 appears in the amplitude because P_{tx} is defined at the passband. Under the PSK assumption, the decision rule takes the form of Eq. (20) with, however, a different threshold [18]:

$$\widetilde{T}_h^{\mathrm{PSK}} = L\,\sigma_0\sigma_1. \tag{23}$$

It can be seen that for both the aforementioned detection schemes, knowledge of $\sigma_{i_\mathrm{n}}^2$ is necessary. A method for estimating those parameters using a short training sequence is provided in [18] and is subsequently utilized in the present work.

B. Detection of Backscatter partially coherent SBPSK

Based on the signal model of Eq. (17), work in [14] proposed an illumination-agnostic, generalized likelihood ratio test (GLRT)-based, partially coherent detection scheme. The coherent part of the scheme corresponds to the estimation of a tag-related parameter, namely Φ_{t}. The detector utilizes the output of two correlators, which operate on the received samples. Assuming perfect synchronization, the correlators' output $r_{\mathrm{n}}^{+}, \ r_{\mathrm{n}}^{-}$ for the nth bit is given by:

$$r_{\mathrm{n}}^{\pm} = \sum_{k=0}^{L-1} \mathrm{y}_{\mathrm{SBPSK}}^{i_\mathrm{n}}[k] \, \mathsf{e}^{\mp \mathrm{j}2\pi F_{\mathrm{sw}} k T_{\mathrm{s}}}. \tag{24}$$

Based on the outputs of the correlators, the following GLRT-based decision rule is obtained [14]:

$$i_\mathrm{n} = \arg \max_{i_\mathrm{n} \in \{0,1\}} |\mathbf{r}_{\mathrm{n}}^H \mathbf{x}_{i_\mathrm{n}}(\Phi_{\mathrm{t}})|^2, \tag{25}$$

where $\mathbf{r}_{\mathrm{n}} = \left[r_{\mathrm{n}}^{+} \ r_{\mathrm{n}}^{-}\right]^{\mathrm{T}}$ and $\mathbf{x}_{i_\mathrm{n}}(\Phi_{\mathrm{t}}) = \left[\mathsf{e}^{\mathsf{j}(\Phi_{\mathrm{t}}+\Phi_{i_n})} \ \mathsf{e}^{-\mathsf{j}(\Phi_{\mathrm{t}}+\Phi_{i_n})}\right]^{\mathrm{T}}$. Defining $\theta_{\mathrm{n}} = \angle(r_{\mathrm{n}}^{+})^{*}(r_{\mathrm{n}}^{-})$, assuming $\Phi_0 = 0$ and $\Delta\Phi = \frac{\pi}{2}$, Eq. (25) is simplified to [14]:

$$\mathsf{cos}(2\Phi_{\mathrm{t}} + \theta_{\mathrm{n}}) \underset{\leq}{\overset{\mathcal{H}_1}{}} 0. \tag{26}$$

Phase Φ_{t} is estimated using a short training sequence (see [14]). It has to be noted that the rule of Eq. (26) is illumination-agnostic, i.e., the derivation of the rule does not assume any specific modulation for the illuminating ambient signal. However, a constraint regarding switching frequency F_{sw} and the illuminating carrier's baseband bandwidth is applied [14].

C. Detection of Backscatter fully non-coherent SBPSK under FM illumination

In order for the detector of Eq. (26) to work, Φ_{t} is required. As stated earlier, phase Φ_{t} is considered random but *constant* throughout the transmission of a specific number of bits. Thus, multiple bits are affected by the same value of Φ_{t}.

As shown in [14], when signal processing using correlators is applied to the received signal and illumination from ambient FM radio stations is considered, coherent detection can be utilized. The feasibility of coherent detection (under FM illumination), dictates that throughout a certain number of bits, the parameters affecting the tag's signal, including the illuminating signal, do not vary significantly. Thus, correlation is introduced between the received statistics. Having stated the above and assuming that the wireless channel parameters also remain constant for a specific number of bits, sequence based detection techniques may be applied.

The following steps are performed to achieve non-coherent detection.

1) The receiver uniformly samples the range $(0, \ldots, 2\pi]$ and acquires M values for Φ_{t}, namely $\tilde{\Phi}_{\mathrm{t},1}, \tilde{\Phi}_{\mathrm{t},2}, \ldots, \tilde{\Phi}_{\mathrm{t},M}$.
2) For each sampled phase $\tilde{\Phi}_{\mathrm{t},k}, \ k \in \{1, \ldots, M\}$, using the detector of Eq. (25) (or Eq. (26)), symbol-by-symbol detection is performed for N bits. That way a total of M N-bit sequences are generated. The kth sequence is acquired as follows:
$$\begin{aligned} i_1^k &= \arg \max_{i \in \{0,1\}} |\mathbf{r}_1^H \mathbf{x}_i(\tilde{\Phi}_{\mathrm{t},k})|^2, \\ &\vdots \\ i_N^k &= \arg \max_{i \in \{0,1\}} |\mathbf{r}_N^H \mathbf{x}_i(\tilde{\Phi}_{\mathrm{t},k})|^2. \end{aligned} \tag{27}$$
3) For each one of the M resulting sequences, receiver stores the value of $\delta_k = |\mathbf{r}_{1:N}^H \, \mathbf{x}_{\mathbf{i}^k}(\tilde{\Phi}_{\mathrm{t},k})|$, where vector definitions follow:
$$\mathbf{r}_{1:N} = \left[\mathbf{r}_1^{\mathrm{T}} \ \mathbf{r}_2^{\mathrm{T}} \ldots \ \mathbf{r}_N^{\mathrm{T}}\right]^{\mathrm{T}} \in \mathbb{C}^{2N}, \tag{28}$$
$$\mathbf{x}_{\mathbf{i}^k}(\tilde{\Phi}_{\mathrm{t},k}) = \left[\mathbf{x}_{i_1^k}^{\mathrm{T}}(\tilde{\Phi}_{\mathrm{t},k}) \ \ldots \ \mathbf{x}_{i_N^k}^{\mathrm{T}}(\tilde{\Phi}_{\mathrm{t},k})\right]^{\mathrm{T}} \in \mathbb{C}^{2N}. \tag{29}$$
4) As a final step, receiver selects the sequence $\mathbf{i}^{k^*} = \left[i_1^{k^*}, \ldots, i_N^{k^*}\right]$ which satisfies:
$$k^* = \arg \max_{k \in \{1, \ldots, M\}} \{\delta_k\}. \tag{30}$$

Given fixed bit duration T_{bit}, sequence length N is selected such that channel coherence time is greater (or equal) than (to) NT_{bit} sec.

IV. Numerical Results

Bit error rate (BER) was considered as the metric of interest. All results are offered using a sequence of $N_{\text{tr}} = 10$ training bits (for parameter estimation) and $N_{\text{d}} = 50$ payload bits. For the case of the fully non-coherent detector, the total payload was $N = N_{\text{d}} = 50$ (no training bits) bits with $M = 50$. Bit duration was fixed through L, which was set to $L = 1000$. Assuming a sampling rate $F_{\text{s}} = 5$ MHz, the chosen value for L represents a bit rate of $R = 1/T_{\text{bit}} = 5$ kbps. Scattering efficiency was set to $\text{s} = \sqrt{0.1}$, while structural mode parameter to $A_{\text{s}} = 0.6047 + \text{j}0.5042$; path-loss exponent was set to $\nu = 2.2$, representing an "optimistic" scenario. The distances were set to $d_{\text{CR}} = 6$ km, $d_{\text{TR}} = 6$ m and $d_{\text{CT}} = d_{\text{CR}} - d_{\text{TR}}$.

Given that the vast majority of literature on theoretical ambient backscatter communication considers as signal-to-noise ratio (SNR) $P_{\text{tx}}/\sigma_{\text{w}}^2$, i.e., the ratio of transmitter's power to the power of complex baseband noise, the carrier-to-noise ratio (CNR) is reported:

$$\text{CNR} \triangleq \frac{P_{\text{rx}}}{\sigma_{\text{w}}^2} = \frac{P_{\text{tx}} L_{\text{CR}} \mathbb{E}\left[|h_{\text{CR}}|^2\right]}{\sigma_{\text{w}}^2} = \frac{P_{\text{tx}} L_{\text{CR}} \sigma_{\text{h}}^2}{\sigma_{\text{w}}^2}. \quad (31)$$

The definition of CNR in Eq. (31) expresses the power ratio of the received ambient carrier signal, from the direct CR link, to the complex baseband noise.

Depending on the scenario, 10^5, 5×10^6 or 8×10^6 Monte Carlo experiments were performed per CNR value. The channel parameters were assumed *constant* for each Monte Carlo run, i.e., for $N_{\text{tr}} + N_{\text{d}} = 60$ bits with $\sigma_{\text{h}}^2 = 1$ and $\text{k}_{\text{TR}} = 20$. It has to be noted that the SBPSK detector (Sec. III-B) can work even when the wireless channel parameters vary between successive bits. Analytical BER expressions are drawn from the results of [18]. Specifically, for CN-derived and PSK-derived detectors, the closed form bit error probability is given by [18, Eq. (10)] and [18, Eq. (47)], respectively. Both expressions require exact knowledge of channel parameters σ_0^2, σ_1^2. Thus, in every Monte Carlo experiment, each expression was evaluated for the experiment's (exact) channel parameters and an average value was obtained at the end of all experiments (averaged over the different channel realizations). That way, an average value for the closed form probability of error is obtained for each CNR.

Illuminating signal was assumed to attain different modulations, namely FM, CN, BPSK and 16-QAM. FM illumination was implemented as $\text{m}_{\text{c}}[k] = \sqrt{2P_{\text{tx}}}\text{e}^{\text{j}\phi_{\text{m}}[k]}$ with $\phi_{\text{m}}[k] \sim \mathcal{N}(0,1)$. For CN illumination, $\text{m}_{\text{c}}[k] \sim \mathcal{CN}(0, 2P_{\text{tx}})$, while BPSK was implemented as per Eq. (22), with $\text{M}_{\text{PSK}} = 2$. For 16-QAM, MATLAB's qammod function was used to obtain the required complex envelope, which was appropriately normalized.

In Fig. 2 the performance of the OOK, CN-derived detector is evaluated for different illuminating conditions; performance

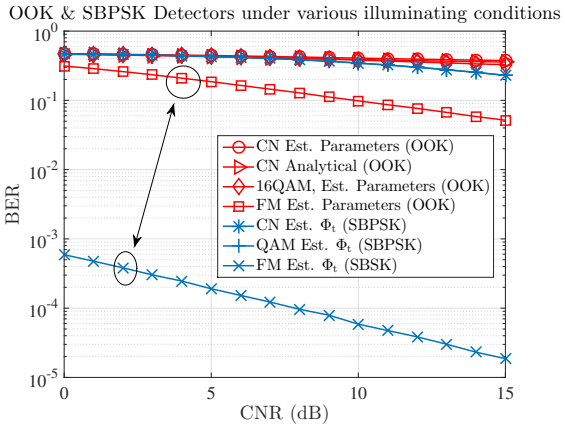

Fig. 2: BER-based evaluation of the OOK (CN-derived, Sec. III-A1) detectors from [18] and SBPSK detectors from [14], under various illuminating conditions (CN, 16-QAM, FM). For 16-QAM and CN illuminations, a carrier frequency of $F_{\text{c}} = 540$ MHz was assumed while for FM, $F_{\text{c}} = 90$ MHz. Carrier's transmit power was set to $P_{\text{tx}} = 4$ kW.

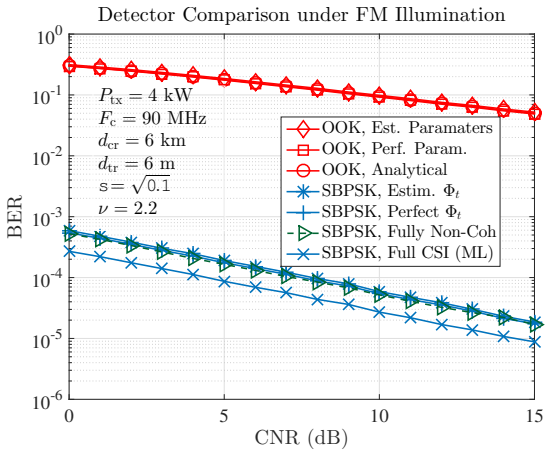

Fig. 3: BER-based evaluation of the OOK (PSK-derived, see Sec. III-A2) detectors from [18] and SBPSK detectors from [14], under FM illumination. SBPSK partially coherent detector is demonstrated for conditions of perfect, estimated Φ_{t} and ML-based full CSI detection. The performance of the proposed fully non-coherent detector, is additionally demonstrated.

of the SBPSK detector is also offered in the same figure. For OOK with CN illumination, the detector of Eq. (20) using perfect and estimated channel parameters σ_0^2, σ_1^2, was evaluated along with the closed form expression for the case ([18, Eq. (10)]). The detector is also evaluated, using parameter estimates, under FM and 16-QAM illumination. Considering CN illumination, the performance of the detectors is similar, with the SBPSK slightly outperforming OOK. However, while for 16-QAM the performance offered by both detectors is identical to CN illumination, if FM illumination is considered, the performance gap compared to CN is significant, for both OOK and SBPSK. The last finding dictates that neglecting the

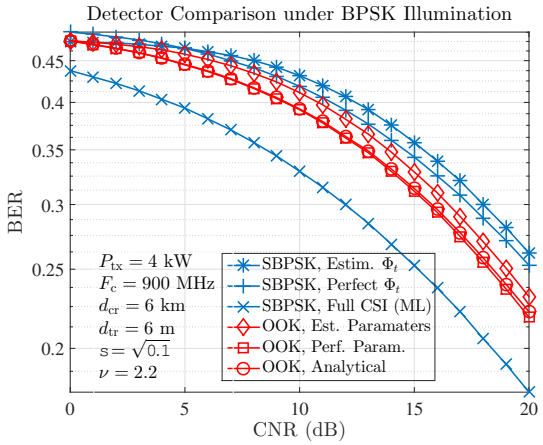

Fig. 4: BER-based evaluation of the OOK (PSK-derived, Sec. III-A2) detectors from [18] and SBPSK detectors from [14], under BPSK illumination. SBPSK partially coherent detector is demonstrated for conditions of perfect, estimated Φ_t and ML-based full CSI detection.

structure of the illuminator's signal, may lead to significant performance loss. It is also observed that SBPSK outperforms OOK when FM illumination is considered. SBPSK is evaluated using an estimate of Φ_t. For the performance of the OOK detectors under simplified signal models, reader is kindly encouraged to see [18].

Performance under FM and BPSK illumination is given in Figs. 3 and 4, respectively. Under FM illumination (Fig. 3) and realistic channel conditions (summarized in the lower left side of the figure), it can be seen that SBPSK detector outperforms OOK. The performance gain is offered at the expense of increased complexity at the tag due to switching during each bit duration (as explained earlier). It can be also seen that the proposed SBPSK-based fully non-coherent detector, performs slightly better than the partially coherent detector, with the latter utilizing perfect information of Φ_t. This behavior can be explained by the nature of the detector, which is sequence-based (Sec. III-C). SBPSK is also evaluated when perfect channel state information (CSI, related to wireless channel, ambient carrier and tag parameters) is available, using an ML detector [14]. Under BPSK illumination (Fig. 4), the OOK scheme with the utilized, PSK-derived, detector outperforms the SBPSK detector. This may be explained by the fact that the considered OOK detector is derived under the assumption of a PSK illuminating signal, while SBPSK detector does not assume any information regarding ambient carrier's modulation. This finding also underlines the importance of the illuminator's signal structure.

V. Conclusion

Through evaluation of recent studies on ambient backscatter, it was shown that switching based techniques (SBPSK) may offer performance gains, compared to conventional schemes (OOK), at the expense of increased tag complexity. The comparison demonstrated that simplified models and assumptions related to carrier's signal structure (e.g., CN illumination), lead to limited performance and shall be dismissed; explicitly taking into account the illuminator's structure (e.g., FM), in conjunction with switching-based schemes, offers improved BER even with fully non-coherent detectors.

VI. Acknowledgment

The research work was supported by the Hellenic Foundation for Research and Innovation (HFRI) and the General Secretariat for Research and Technology (GSRT), under the HFRI PhD Fellowship grant (GA. no. 2263).

References

[1] G. Vannucci, A. Bletsas, and D. Leigh, "A software-defined radio system for backscatter sensor networks," *IEEE Trans. Wireless Commun.*, vol. 7, no. 6, pp. 2170–2179, Jun. 2008.

[2] J. Kimionis, A. Bletsas, and J. N. Sahalos, "Increased range bistatic scatter radio," *IEEE Trans. Commun.*, vol. 62, no. 3, pp. 1091–1104, Mar. 2014.

[3] P. N. Alevizos, K. Tountas, and A. Bletsas, "Multistatic scatter radio sensor networks for extended coverage," *IEEE Trans. Wireless Commun.*, vol. 17, no. 7, pp. 4522–4535, Jul. 2018.

[4] V. Liu, A. Parks, V. Talla, S. Gollakota, D. Wetherall, and J. R. Smith, "Ambient backscatter: Wireless communication out of thin air," in *Proc. ACM SIGCOMM*, Hong Kong, China, 2013, pp. 39–50.

[5] A. Wang, V. Iyer, V. Talla, J. R. Smith, and S. Gollakota, "FM backscatter: Enabling connected cities and smart fabrics," in *USENIX Symp. on Networked Systems Design and Implementation*, Boston, MA, USA, Mar. 2017.

[6] G. Vougioukas and A. Bletsas, "24μW 26m range batteryless backscatter sensors with FM remodulation and selection diversity," in *Proc. IEEE RFID Techn. and Applications (RFID-TA)*, Warsaw, Poland, Sep. 2017.

[7] G. Yang, Y. Liang, R. Zhang, and Y. Pei, "Modulation in the air: Backscatter communication over ambient ofdm carrier," *IEEE Trans. Commun.*, vol. 66, no. 3, pp. 1219–1233, Mar. 2018.

[8] G. Wang, F. Gao, R. Fan, and C. Tellambura, "Ambient backscatter communication systems: Detection and performance analysis," *IEEE Trans. Commun.*, vol. 64, no. 11, pp. 4836–4846, Nov. 2016.

[9] J. Qian, F. Gao, G. Wang, S. Jin, and H. Zhu, "Noncoherent detections for ambient backscatter system," *IEEE Trans. Wireless Commun.*, vol. 16, no. 3, pp. 1412–1422, Mar. 2017.

[10] J. Qian, A. N. Parks, J. R. Smith, F. Gao, and S. Jin, "Iot communications with m-psk modulated ambient backscatter: Algorithm, analysis, and implementation," *IEEE Internet of Things J.*, pp. 1–1, 2018.

[11] N. Van Huynh, D. T. Hoang, X. Lu, D. Niyato, P. Wang, and D. In Kim, "Ambient Backscatter Communications: A Contemporary Survey," Dec. 2017. [Online]. Available: https://arxiv.org/abs/1712.04804

[12] A. Bletsas, P. N. Alevizos, and G. Vougioukas, "The art of signal processing in backscatter radio for μW (or less) internet of things: Intelligent signal processing and backscatter radio enabling batteryless connectivity," *IEEE Signal Processing Mag.*, vol. 35, no. 5, pp. 28–40, Sep. 2018.

[13] N. Fasarakis-Hilliard, P. N. Alevizos, and A. Bletsas, "Coherent detection and channel coding for bistatic scatter radio sensor networking," *IEEE Trans. Commun.*, vol. 63, pp. 1798–1810, May 2015.

[14] G. Vougioukas and A. Bletsas, "Switching frequency techniques for universal ambient backscatter networking," *IEEE J. Select. Areas Commun.*, vol. 37, no. 2, pp. 464–477, Feb. 2019.

[15] N. Weste and D. Harris, *CMOS VLSI Design: A Circuits and Systems Perspective*, 4th ed. USA: Addison-Wesley Publishing Company, 2010.

[16] P. N. Alevizos, A. Bletsas, and G. N. Karystinos, "Noncoherent short packet detection and decoding for scatter radio sensor networking," *IEEE Trans. Commun.*, vol. 65, no. 5, pp. 2128–2140, May 2017.

[17] A. Goldsmith, *Wireless Communications*. New York, NY, USA: Cambridge University Press, 2005.

[18] J. Qian, F. Gao, G. Wang, S. Jin, and H. Zhu, "Semi-coherent detection and performance analysis for ambient backscatter system," *IEEE Trans. Commun.*, vol. 65, no. 12, pp. 5266–5279, Dec. 2017.